Nanosized MX Precipitates in Ultra-Low-Carbon Ferritic/Martensitic Heat-Resistant Steels

FENG-SHI YIN and WOO-SANG JUNG

Nanosized MX precipitates in ultra-low-carbon ferritic/martensitic heat-resistant 9Cr-W-Mo-VNbTiN steels were characterized by transmission electron microscope (TEM) using carbon film replicas. The steels were prepared by vacuum induction melting followed by hot forging and rolling into plates. The plates were normalized at 1100 °C for 1 hour, cooled in air, and tempered at 700 °C for 1 hour. The results show that bimodal nanosized MX precipitates distribute densely and homogeneously in the matrix within martensitic lath after normalizing-and-tempering heat treatment. The larger nanosized MX precipitates with the size of 30 to 50 nm are rich in Nb, while the smaller ones with the size of about 10 nm contain less Nb but more V. Small addition of Ti causes an increase in the number of the larger nanosized MX precipitates. The total number density of the nanosized MX precipitates in the ultra-low-carbon ferritic/martensitic steels is measured to be over $300/\mu m^2$, much higher than that in conventional ferritic/martensitic steels. Short-term creep test results show that the ultra-low-carbon ferritic/martensitic steels with high dense nanosized MX precipitates have much higher creep rupture strength than conventional ASME-P92 steel. The strength degradation of the ultra-low-carbon ferritic/martensitic heat-resistant steels during creep is also discussed in this article.

DOI: 10.1007/s11661-008-9716-x

I. INTRODUCTION

REDUCTION of CO_2 emission is an urgent task for power industries, especially for fossil power plants. The amount of CO_2 emission decreases with increasing operation temperature of the plants. Plant operation at higher temperature requires heat-resistant materials with higher creep strength. 9-12Cr ferritic/martensitic heat-resistant steels have been widely used in fossil power plants, because those steels have high thermal conductivity and low thermal expansion coefficient, and they also possess less susceptibility to the thermal fatigue than austenitic stainless steel.[1–7] In order to increase creep strength, these steels are strengthened by various strengthening mechanisms such as solution hardening by Mo or W, particle hardening by MX within subgrains, particle hardening due to particles ($M_{23}C_6$ and Fe_2W) on sub-boundaries, as well as dislocation hardening.[1] The precipitation strengthening is the most effective mechanism for conventional 9-12Cr steels. In particular, MX-type carbonitrides, which are composed of vanadium, niobium, and so on, and precipitate finely and densely in the matrix of the steels, increase creep strength significantly.[4,7]

Hasegawa *et al.*[6] analyzed the precipitation behavior and morphology of nanosized precipitates in ASME Gr. 92 (9 pct Cr-1.8 pct W-MoNbVNB) by transmission electron microscope (TEM) observation and characterization of precipitates. Granular or tabular MX precipitates and composite MX precipitates called V-wing were found in ASME Gr. 92 steel. The average particle size of the MX precipitates as measured with an energy-filtered TEM is, reportedly, 20 to 50 nm. Taneike *et al.*[7] reported that extremely low-carbon 9Cr ferritic steel (9Cr-3W-0.2V-0.06Nb-3Co-0.05N-B) exhibits much higher creep strength than 9Cr-0.5Mo-1.8W-VNbN (ASME-P92) steel does. By reducing the carbon content of the ferritic steel, not the $M_{23}C_6$ carbides but only fine MX nitrides precipitate along lath, block, packet, and prior austenite grain boundaries as well as in the matrix during tempering. The fine MX nitride can pin the boundaries during long-term creep deformation, because the growth rate of the MX nitride is much lower than that of the $M_{23}C_6$ carbide. In our previous investigation, nanosized MX precipitates were found to distribute densely and homogeneously in the matrix within martensitic lath after normalizing-and-tempering heat treatment in an ultra-low-carbon ferritic/martensitic heat-resistant steel with 9.37Cr, 3.2W, 4.0Co, 0.22V, 0.09Nb, 0.068N, and 0.007Ti (in mass pct).[8] The time to rupture at 650 °C under high stress for the ultra-low-carbon steel is much longer than that for the conventional ASME-P92 steel due to the strengthening effect caused by the dense and homogeneous nanosized MX precipitates. However, the strength degradation for the ultra-low-carbon steel during long-time creep is faster, and the time to rupture is expected to be shorter than that for the ASME-P92 steel under low stress.

In this article, the nanosized MX precipitates in three ultra-low-carbon ferritic/martensitic steels were

FENG-SHI YIN, Professor, is with the School of Mechanical Engineering, Shandong University of Technology, Zibo 255049, P.R. China. Contact e-mail: fsyin@sdut.edu.cn WOO-SANG JUNG, Principal Researcher, is with the Division of Materials Science and Technology, Korea Institute of Science and Technology, Cheongryang, Seoul 130-650, Korea.

Manuscript submitted March 3, 2008.
Article published online December 17, 2008

characterized in detail by TEM using carbon film replicas. The effect of composition on microstructure and mechanical properties of the ultra-low-carbon ferritic/martensitic steels were studied.

II. EXPERIMENTAL

The composition of the ultra-low-carbon steels used in this study is shown in Table I. In order to restrain the formation of δ ferrite, cobalt was added to the steels. A small amount of titanium was also used to further stabilize the nanosized MX phase. Hot forging and rolling were performed to produce 10-mm-thick plates. The heating temperature before forging and rolling, respectively, was 1100 °C. The plates were normalized at 1100 °C for 1 hour, cooled in air, and then tempered at 700 °C for 1 hour. Specimens of 4 mm in gage diameter and 25 mm in gage length were machined from the normalized-and-tempered plates with the specimen axis parallel with the rolling direction. Creep tests were conducted in air at 650 °C/300, 250, 200 MPa and 700 °C/170, 140, 110 MPa. The normalized-and-tempered steels were also aged at 650 °C for up to 5240 hours in air.

Microstructures of the specimens were characterized by a Hitachi (Tokyo, Japan) S-4100 field emission scanning electron microscope. Precipitate microstructures were observed and identified by both a PHILIPS* CM30 TEM and an FEI Techai (FEI Co., Eindhoven, Netherlands) 20 TEM using carbon film replicas. Both TEMs are equipped with energy dispersive spectrum analysis (EDS). X-ray diffraction (XRD) of electrolytic extraction residues was used to examine the change in precipitates during long-term exposure and to compare the difference among the steels studied. The extracted residues were prepared by using ethanol with 10 vol pct hydrochloric acid.

*PHILIPS is a trademark of Philips Electronic Instruments Corp., Mahwah, NJ.

III. RESULTS

A. *Microstructure after Normalizing-and-Tempering Heat Treatment*

The SEM observation shows that the microstructures of the ultra-low-carbon ferritic/martensitic steels after normalizing-and-tempering heat treatment are all tempered lath martensite, as reported in elsewhere.[8] The $M_{23}C_6$ precipitate, which is the dominant precipitate in conventional 9Cr ferritic/martensitic steels, is hardly found in these ultra-low-carbon steels (Figure 1).

The TEM observation demonstrates that bimodal nanosized MX precipitates distribute in the matrix of the ultra-low-carbon ferritic/martensitic steels at the normalized-and-tempered state. Figure 2 shows the typical TEM micrographs and selected area diffraction pattern (SADP) obtained by the PHILIPS CM30 TEM from the carbon film replica of steel A at the normalized-and-tempered state. A pattern with spots and ring is obtained (Figure 2(b)). The spot pattern corresponds to the larger MX precipitates with the size of 30 to 50 nm (Figure 2(c)), and the diffraction ring corresponds to the smaller one with the size of about 10 nm. Figure 2(d) shows the dark-field image of the smaller MX precipitates. It can be seen that the smaller nanosized MX precipitates distribute densely and homogeneously in the matrix within the martensitic lath. The EDS result indicates that the larger nanosized MX precipitates are rich in Nb, as shown in Figure 2(e). The smaller nanosized MX precipitates are too small to be determined by the PHILIPS CM30 TEM-EDS analysis. Figure 3 shows a typical smaller nanosized MX precipitate and its EDS spectrum obtained by a high-resolution TEM, the FEI Techai 20 TEM. In contrast to the larger nanosized MX, the smaller one contains less Nb but more V. Small amounts of Cr and Fe are also detected in the EDS results.

Figures 4(a) and (b) show the low-magnification TEM images of the carbon film replica for steel B at both the normalized-and-tempered state and the normalized state, respectively. The larger nanosized MX precipitates are present in the steels both at normalized

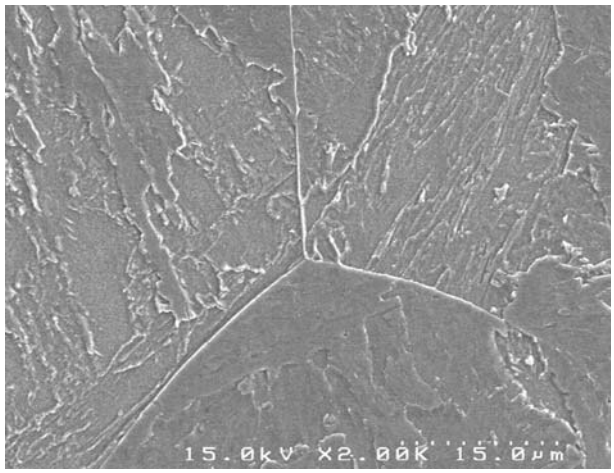

Fig. 1—SEM secondary electron micrograph of steel A after normalizing-and-tempering heat treatment.

Table I. Composition of the Ultra-Low-Carbon Ferritic/Martensitic Heat-Resistant Steels

Alloy	C	Si	Mn	Cr	Ni	Mo	W	Co	V	Nb	Ti	B	N
Steel A	0.001	0.16	0.03	9.2	0.05	0.55	1.9	4.0	0.21	0.09	0.003	0.0007	0.055
Steel B	0.001	0.17	0.04	9.3	0.05	0.55	1.9	4.0	0.21	0.09	0.007	0.0005	0.064
Steel C	0.001	0.16	0.03	9.4	0.05	0.09	3.2	4.0	0.22	0.09	0.006	0.0011	0.068

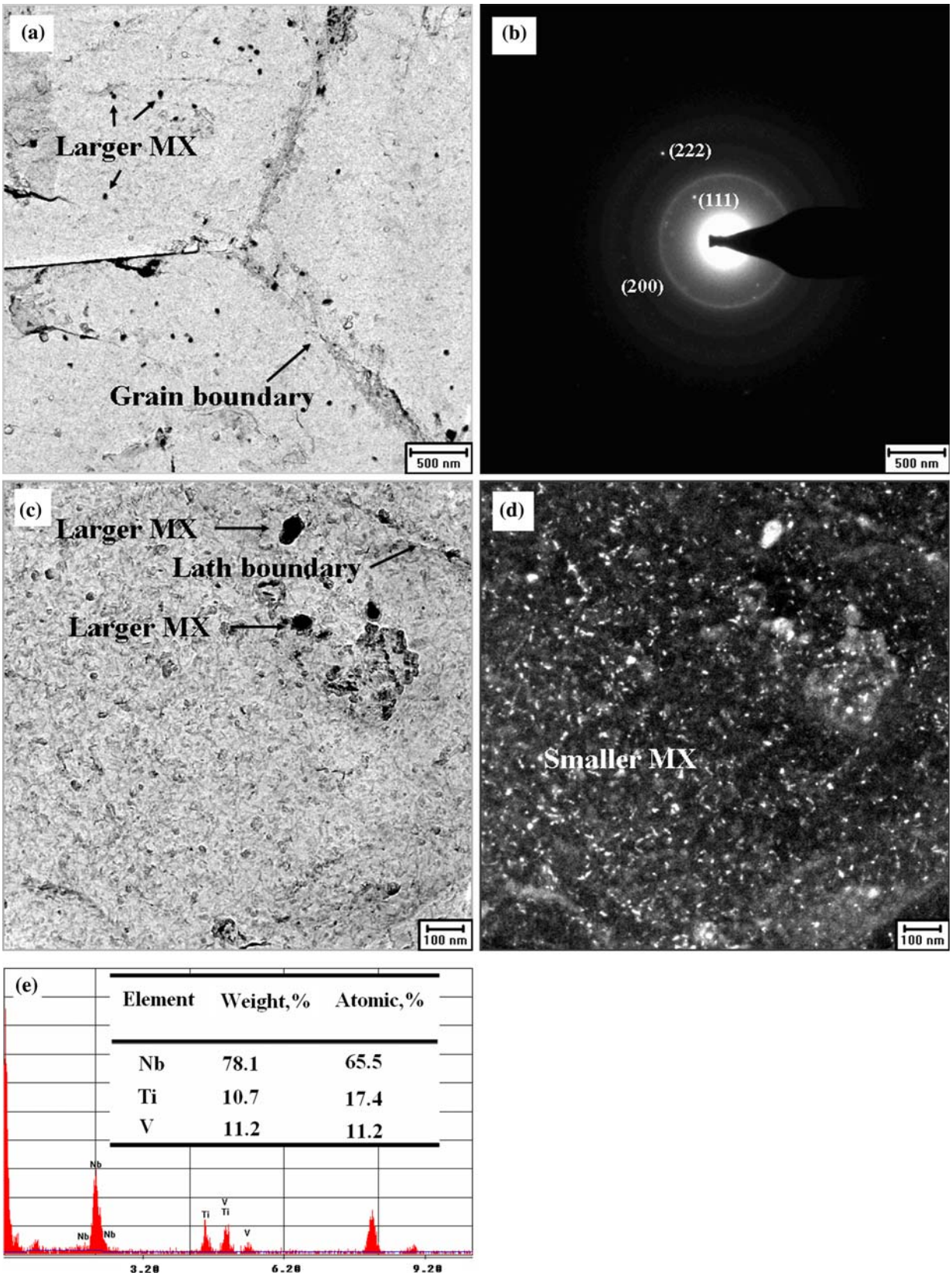

Fig. 2—TEM images of carbon film replica for steel A at normalized-and-tempered state obtained by a PHILIPS CM30 TEM. (*a*) low magnification; (*b*) diffraction patterns in which the spot pattern corresponds to the larger MX with the size of 30 to 50 nm and the diffraction rings to the smaller MX with the size of less than 10 nm; (*c*) bright-field image in high magnification; (*d*) dark-field image in high magnification; and (*e*) EDS result of the larger nanosized MX.

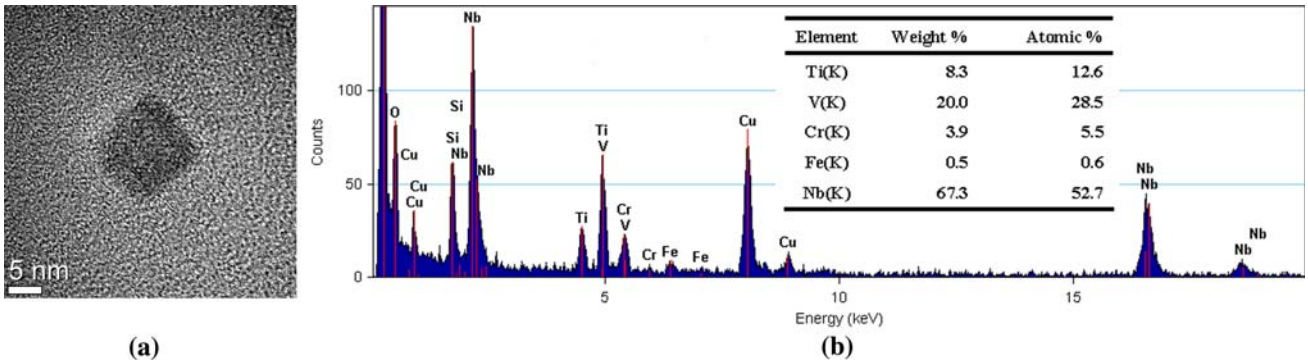

Fig. 3—Smaller nanosized MX obtained by a FEI Techai 20 TEM: (*a*) high-resolution TEM image and (*b*) EDS result.

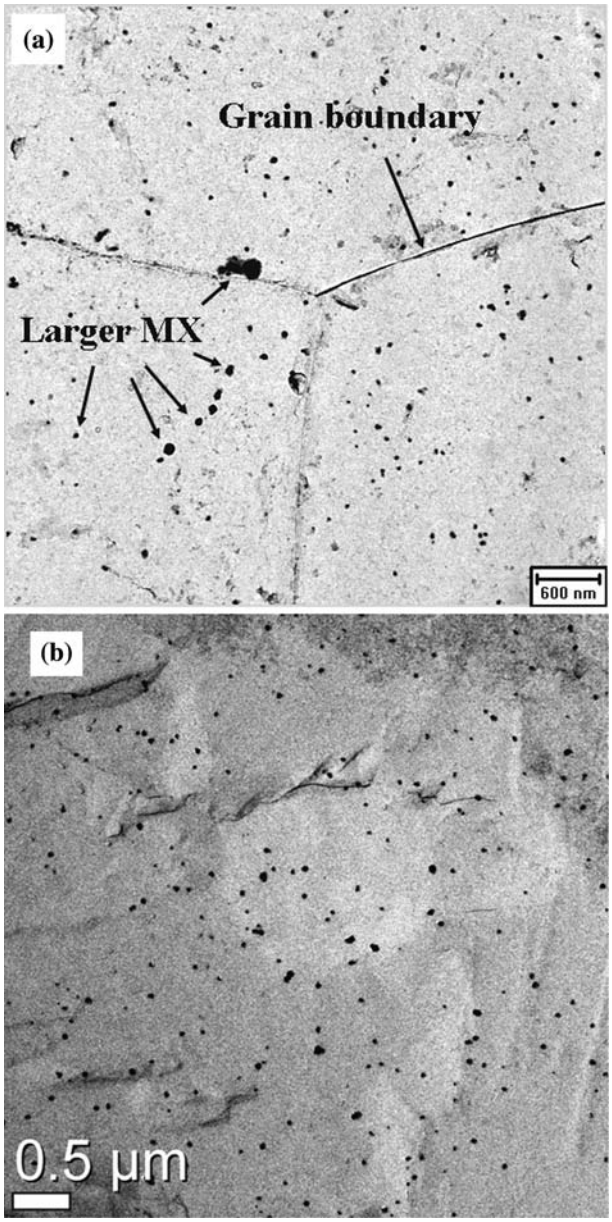

Fig. 4—TEM images of carbon film replica for steel B at (*a*) normalized-and-tempered state and (*b*) normalized state.

Table II. Density of Nanosized MX Precipitates

Alloy	Larger Nanosized MX $N/\mu m^{-2}$	Smaller Nanosized MX $N/\mu m^{-2}$	Orowan Stress σ_{Or}/MPa
Steel A	2.50	546	672
Steel B	5.48	388	566
Steel C	7.29	304	501

state and normalized-and-tempered state, indicating that the larger nanosized MX precipitates already exist before and do not dissolve during the normalizing heat treatment adopted in the present study. In contrast with Figure 2(a), it is found that the number density of the larger MX precipitates in steel B is higher than that in steel A. The measured number density of both the larger and smaller nanosized MX precipitates in these three steels is summarized in Table II. In steel A, with the lowest Ti and nitrogen contents, the number density of the smaller nanosized MX is higher than that in steel B or steel C while the number density of the larger nanosized MX is the lowest, which means that the small increase in Ti content causes an increase in the number of the larger nanosized MX precipitates; accordingly, the number of the smaller nanosized MX precipitates is decreased. Comparing steel C with steel B, only a little difference in number density of the nanosized MX precipitates is found, as shown in Table II. The difference in tungsten content does not cause much difference in microstructure in the normalized-and-tempered state between steels B and C.

B. *Creep Properties*

Figure 5 shows the relationship between the stress and time to rupture for the ultra-low-carbon ferritic/martensitic steels at 650 °C. For comparison, the creep data from Reference 7 for the conventional ASME-P92 steel at 650 °C is also included in this figure. It is shown that the ultra-low-carbon ferritic/martensitic steels with high dense nanosized MX precipitates have much higher creep rupture strength than conventional ASME-P92 steel under the short time creep conditions. However, it must be noted that the slope of the plots for the

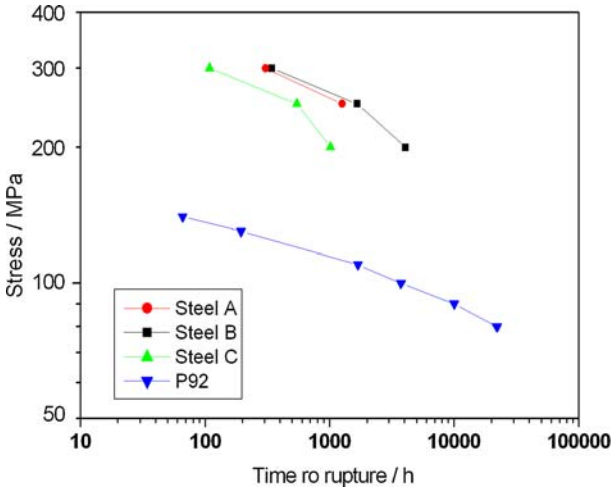

Fig. 5—Stress and time to rupture relationship for the present steels at 650 °C.

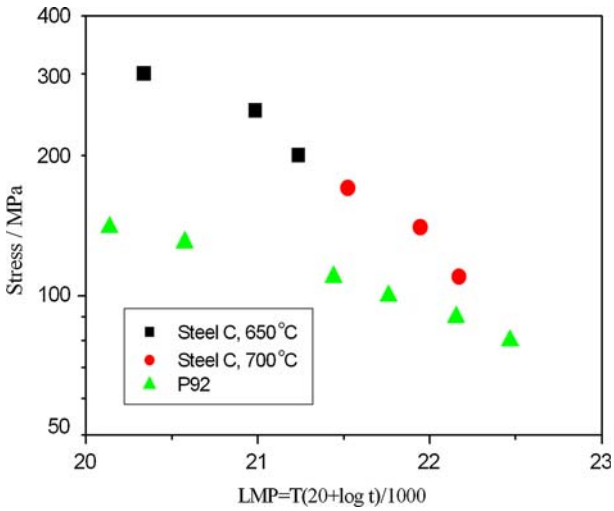

Fig. 6—Larson–Miller plot for steel C and ASME-P92.

ultra-low-carbon steels is steeper than that for the ASME-P92 steel, especially for steel C with high tungsten content and the highest nitrogen content, which indicates that the strength degradation for the ultra-low-carbon steels during long-time creep is faster and the time to rupture might be shorter than that for the ASME-P92 steel under low stress, which is rather unexpected.

Figure 6 shows the creep rupture stress for steel C as a function of the Larson–Miller parameter, $T(C + \log t)$, where T is the absolute temperature, t is the rupture hours, and C is a constant, here, $C = 20$. It is obvious that the slope of the plots for the ultra-low-carbon steel is much steeper than that for the ASME-P92 steel.

C. *The Change in Precipitates during Long-Time Aging at 650 °C*

Figure 7 shows the XRD patterns of electrolytic residues from steel C in the as-tempered state and aged

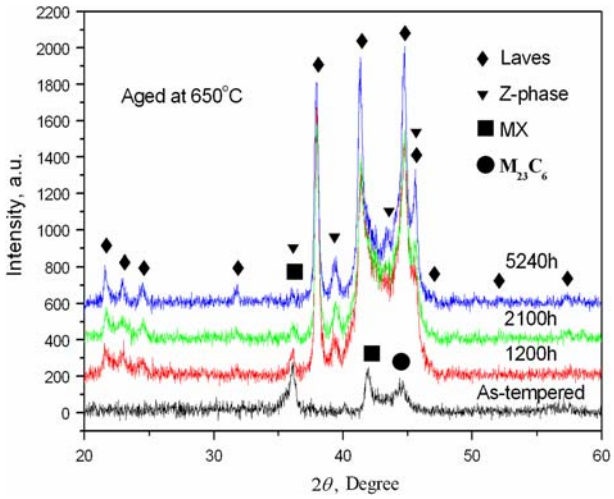

Fig. 7—XRD patterns of electrolytic residues from steel C in as-tempered state and aged at 650 °C for 1200, 2100, and 5240 h.

at 650 °C for 1200, 2100, and 5240 hours. In the as-tempered state, the total amount of residues is very small, less than 0.3 wt pct. The dominating precipitate in steel C is MX phase in the as-tempered state. Because the steel has ultra-low-carbon content, only a weak peak from $M_{23}C_6$ phase is detected in the as-tempered state. After aging at 650 °C for 1200 hours, Fe_2W-type Laves phase becomes the dominating precipitate. Besides Laves phase, Z phase, which is composed of Cr, V, and Nb and reported by Strang *et al.*,[9] is also detected. When the aging time is prolonged, the peaks of Z phase become higher and higher.

Figure 8(a) shows the TEM image of the carbon film replica for steel C aged at 650 °C for 2100 hours. The EDS results of several selected particles are summarized in Table III. Figure 8(b) shows the EDS spectrum of particle B. Particles A, B, and C are composed of Cr, V, Nb, and a small amount of Fe, indicating that they are Z phase formed during long-term aging. The SADP of particle B (Figure 8(c)) confirms that these Cr, V, and Nb containing particles are Z phase, having a tetragonal unit cell with $a = 0.286$ nm and $c = 0.739$ nm. Particle D is composed of Fe, W, Cr, and Mo and is believed to be Laves phase. Laves phase precipitates during long-term aging and grows fastest among all the precipitates. Particle E is mainly composed of Nb and V, indicating that it is the larger nanosized MX, as mentioned previously. A small amount of Cr and Fe in the EDS result of particle E is believed to come from other particles around it. It is also seen that the Z phase is larger than MX particles, indicating that the growth rate of Z phase is very quick.

Figures 9 and 10 show the XRD patterns of electrolytic extraction residues from steels A, B, and C aged at 650 °C for 2100 and 5240 hours, respectively. The Z phase is not detected in steels A and B before aging at 650 °C for 2100 hours, but is detected after aging at 650 °C for 5240 hours. The results indicate that it is easy to form Z phase in steel C than in steels A and B during long-term aging at 650 °C. Even though the

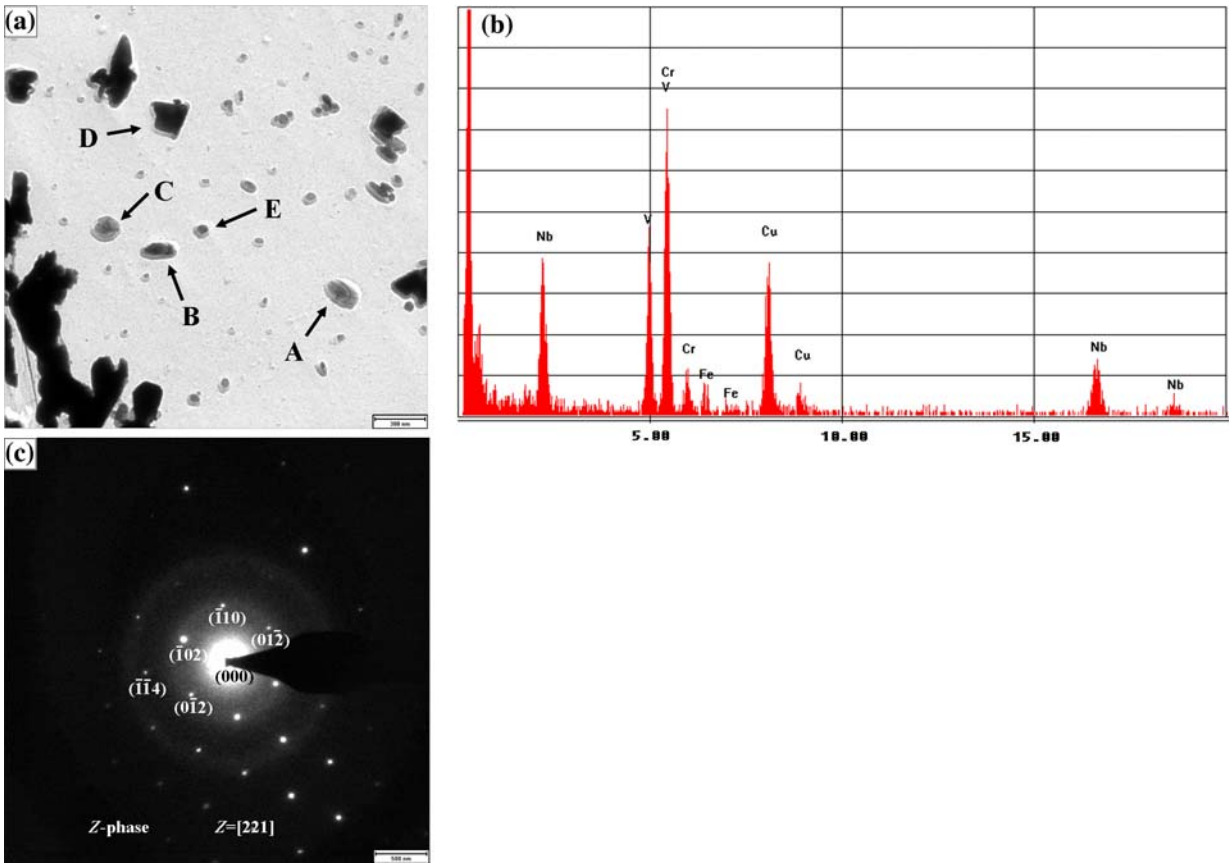

Fig. 8—TEM image of carbon film replica for steel C aged at 650 °C for 2100 h showing *Z* phase particles marked by arrows A, B and C in (*a*). (*b*) EDS spectrum of particle B. (*c*) SADP of particle B. The *Z* phase has a tetragonal unit cell with $a = 2.86$ nm and $b = 7.39$ nm.

Table III. EDS Results of Several Selected Particles in Figure 8 in Atomic Percent

Particle	V	Nb	Cr	Fe	W	Mo	Precipitate
A	19.3	34.4	38.9	7.4	0	0	*Z* phase
B	25.7	21.9	48.2	4.2	0	0	*Z* phase
C	24.7	24.1	46.1	5.1	0	0	*Z* phase
D	0	0	15.3	42.2	41.0	1.6	Laves
E	14.3	80.9	3.1	1.7	0	0	MX

microstructures of steel C in the as-tempered state are similar to those of steel B, the rate of *Z* phase formation in steel C during long-term aging is much faster than the rate of *Z* phase formation in steel B.

IV. DISCUSSION

The present result is different from the previous one reported by Taneike *et al.*[7] They examined 9Cr-3W-3Co-0.2V-0.05N steels with different carbon contents and found a high density of 5 to 10 nm MX precipitates on or in the vicinity of prior-austenite and lath boundaries for 0.002 pct C after normalizing and tempering treatment. However, the nanosized MX precipitates in the present ultra-low-carbon steels are homogeneously distributed in the matrix within the lath, as shown in Figure 2(d). This is due to the low tempering temperature. In the present study, the tempering temperature is 700 °C, lower than the tempering temperature (800 °C) adopted in Reference 7. Because the tempering temperature is low, the steels have many more excess dislocations within the martensitic structure, which increase the nucleation rate of MX precipitates.

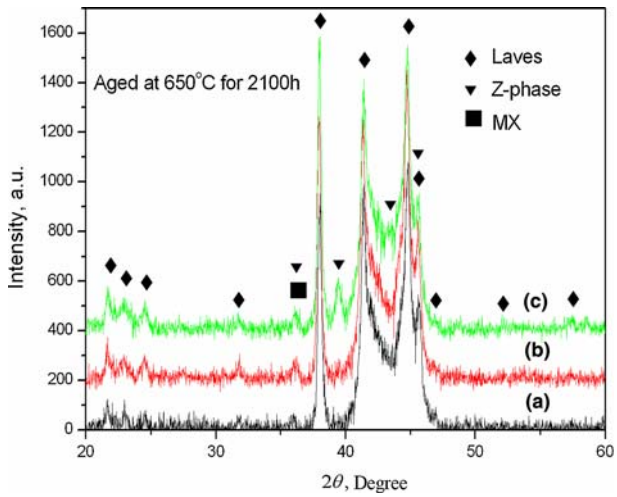

Fig. 9—XRD patterns of electrolytic extraction residues from (*a*) steel A, (*b*) steel B, and (*c*) steel C aged at 650 °C for 2100 h.

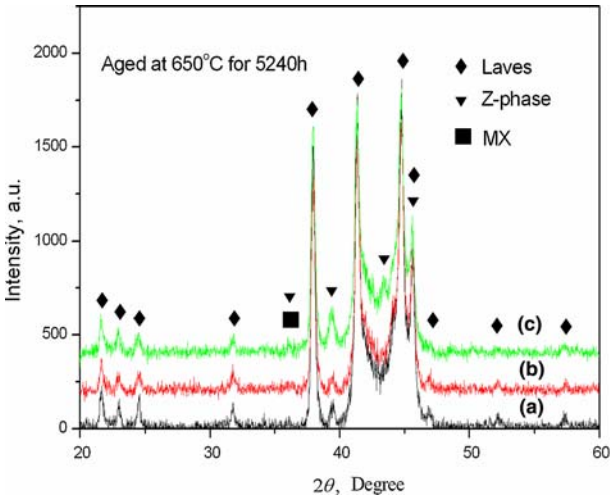

Fig. 10—XRD patterns of electrolytic extraction residues from (*a*) steel A, (*b*) steel B, and (*c*) steel C aged at 650 °C for 5240 h.

The present results show that bimodal nanosized MX precipitates distribute in the matrix of these three ultra-low-carbon steels, and the larger MX is Nb-rich nitride and contains a small amount of titanium. It is well known that both NbN and TiN are more stable than VN. TiN, in particular, is extremely stable up to the melting temperature.[5] The addition of Ti to the ultra-low-carbon steels makes NbN more stable. Therefore, the larger MX is the remaining one that cannot be dissolved completely during the normalizing heat treatment adopted in the present study. Increasing the Ti content causes the increase in number density of the larger MX particles. The number density of larger nanosized MX particles is a little high in steel C as compared to steel B, though titanium is the same in both steels. This is because the nitrogen content is a little higher in steel C than in steel B. Small amounts of Cr and Fe are also detected in the EDS results. They may come from the Cr and Fe containing particles around the smaller nanosized MX particle.

We should point out that the compositions of different smaller nanosized precipitates might be very different. Those steels have 0.2 wt pct V and 0.09 wt pct Nb; however, the EDS results of both larger and smaller nanosized precipitates detected all reveal that the Nb content is higher than the V content. The possible reason is that some much smaller nanosized precipitates have more V than Nb; however, they are too small for us to obtain their EDS spectra.

It is easy to understand that the ultra-low-carbon ferritic/martensitic steels with high dense nanosized MX precipitates have much higher creep rupture strength than conventional ASME-P92 steel. The Orowan stress σ_{Or} for these three steels, given by the following equation, is summarized in Table II:

$$\sigma_{Or} = M G \mathbf{b}/\lambda$$

where M is the Taylor factor (M = 2), G is the shear modulus ($G = 5.8 \times 10^4$ MPa at 650 °C), $\mathbf{b}$ is the length of the Burgers vector ($\mathbf{b}$ = 0.248 nm), and λ is the mean interparticle spacing. The following equation correlates λ to the number density N of the nanosized MX precipitates:

$$N = 1/\lambda^2$$

It is unexpected that the strength degradation for the present steels is faster than that for the ASME-P92 steel. In our previous study, it was suggested that the lower tempering temperature and high nitrogen concentration, as well as the existence of oxide inclusions and coarse nitride particles, are the main reasons for the fast degradation in strength of steel C during long-time creep.[8] The lower tempering temperature can cause fast strength degradation, because the excess dislocations within martensitic structure accelerate the recovery and recrystallization during creep.[11] The coarsening rate of MX nitrides was larger in the high nitrogen 0.07N and 0.10N steels than in the low nitrogen 0.05N steel, and the precipitation of Z phase, Cr(V, Nb)N, took place at shorter times in the high nitrogen steels than in the low nitrogen steels.[10]

In the present study, TEM observation on a specimen aged at 650 °C for 2100 hours reveals the formation of Laves and Z phases in steel C, as shown in Figure 8. The Laves-phase particles formed during creep have large size of about 300 to 500 nm and low number density of about 0.35/μm^2. Therefore, their contribution to strength is very small as compared to the nanosized MX precipitation strengthening. Because the Z phase contains the same constituents V and Nb as the MX carbonitrides, its precipitation is accompanied by dissolution of the beneficial MX particles, especially the smaller nanosized MX particles. After aging at 650 °C for 2100 hours, it becomes impossible to obtain a dark-field image of nanosized MX precipitates, because their number density is decreased greatly. The Z phase precipitates, because they are relatively large particles, do not contribute to particle strengthening. Accordingly, the creep strength of the steel containing large Z phase particles is considerably reduced as compared to the same steel containing MX carbonitrides.[10,12,13]

The Z phase formation takes place much earlier in the present ultra-low-carbon steels, especially in the high W containing steel, the steel C, than in conventional 9Cr steels, such as ASTM-P92 steel, in which it takes place after creep at 873 K for nearly 40,000 hours.[14] It is well known that the Cr and N are the Z phase formation elements. However, the Cr and N contents have little difference between the present ultra-low-carbon steels and ASTM-P92 steel. It is not clear now whether the higher tungsten content can accelerate Z phase formation. The possible reason why Z phase formation is much earlier in the present ultra-low-carbon steels might be as follows: Conventional 9Cr steels contain about 0.1 wt pct carbon, which is combined with Cr to form $M_{23}C_6$ carbide during the tempering treatment and results in the decrease in Cr content in the matrix. The 0.1 wt pct carbon can consume about 1.5 wt pct Cr to form $M_{23}C_6$ carbide if $M_{23}C_6$ contains 21/23 Cr atoms

of total metal elemental atoms. However, in the present ultra-low-carbon steels, the $M_{23}C_6$ carbide is hardly found, and the Cr content in the matrix cannot be decreased by the precipitation of $M_{23}C_6$ carbide. Therefore, the *Z* phase is easy to form in the present ultra-low-carbon steels. As for steel C, because it contains 3.2 wt pct W, higher than that in steel A or B, more Laves precipitates form at the early stage of creep or aging treatment in it than in steel A or B. The formation of Laves phase results in the increase in Cr content around the Laves phase, where *Z* phase will form easily.

V. CONCLUSIONS

Bimodal nanosized MX precipitates have been observed to distribute densely and homogeneously in the matrix within martensitic lath after normalizing-and-tempering heat treatment in the present ultra-low-carbon steels. The larger nanosized MX precipitates with the size of 30 to 50 nm are rich in Nb, while the smaller ones with the size of about 10 nm contain less Nb but more V. A small addition of Ti causes an increase in the number of the larger nanosized MX precipitates. The total number density of the nanosized MX precipitates in the ultra-low-carbon ferritic/martensitic steels is measured to be over $300/\mu m^2$, much higher than that in conventional ferritic/martensitic steels. The ultra-low-carbon ferritic/martensitic steels with high dense nanosized MX precipitates have much higher creep rupture strength than conventional ASME-P92 steel in the short-term creep test at 650 °C.

ACKNOWLEDGMENTS

Financial support from the National Natural Science Foundation of China (Grant No. 50771059) and start-up scientific research fund for oversea returned talents sponsored by the Ministry of Education is acknowledged.

REFERENCES

1. K. Maruyama, K. Sawada, and J.-I. Koike: *ISIJ Int*., 2001, vol. 41, pp. 641–53.
2. P.J. Ennis and A. Czyrska-Filemonowicz: *OMMI*, 2002, vol. 1, pp. 1–28, available at www.ommi.co.uk.
3. R. Blum and R.W. Vanstone: *Proc. 6th Int. Charles Parsons Turbine Conf*., Dublin, Ireland, Sept. 16–18, Institute of Materials, Minerals, and Mining, London, UK, 2003, pp. 489–510.
4. M. Taneike, N. Fujitsuna, and F. Abe: *Mater. Sci. Technol*., 2004, vol. 20, pp. 1455–61.
5. F. Abe, M. Taneike, and K. Sawada: *Int. J. Press. Vess. Piping*, 2007, vol. 84, pp. 3–12.
6. Y. Hasegawa, T. Muraki, S. Yoshida, M. Ohgami, Y. Okayama, F. Kawazoe, and S. Umeki: Nippon Steel Technical Report No. 91, Nippon Steel, Tokyo, Japan, Jan. 2005.
7. M. Taneike, F. Abe, and K. Sawada: *Nature*, 2003, vol. 424, pp. 294–98.
8. F.-S. Yin, W.-S. Jung, and S.-H. Chung: *Scripta Mater*., 2007, vol. 57, pp. 469–72.
9. A. Strang and V. Vodarek: *Mater. Sci. Technol*., 1996, vol. 12, pp. 552–56.
10. K. Sawada, M. Taneike, K. Kimura, and F. Abe: *ISIJ Int*., 2004, vol. 44, pp. 1243–49.
11. A. Iseda, H. Teranishi, and F. Masuyama: *Tetsu-to-Hagané*, 1990, vol. 76, pp. 1076–83.
12. H.K. Danielsen and J. Hald: *Energy Mater*., 2006, vol. 1, pp. 49–57.
13. H.K. Danielsen and J. Hald: *Calphad*, 2007, vol. 31, pp. 505–14.
14. K. Sawada, H. Kushima, and K. Kimura: *ISIJ Int*., 2006, vol. 46, pp. 769–75.